

Beamforming of the Residuals is the LASSO's Dual

Christoph F. Mecklenbräuer, Peter Gerstoft, Erich Zöchmann

Abstract

Waves hidden in additive noise are observed by a sensor array. The waves are assumed to originate from a sparse set of sources. We treat the estimation of the sparse set of sources as a generalized complex-valued LASSO problem. The generalized complex-valued LASSO problem is strictly convex and strong duality holds. The corresponding dual problem is interpretable as a weighted conventional beamformer acting on the residuals of the LASSO. Moreover, this establishes a simple linear-affine relation between the dual and primal vectors. The solution path of the complex-valued LASSO is analyzed and three procedures for signal processing are proposed and evaluated which are based on the generalized LASSO and its dual: An order-recursive procedure and two iterative procedures which are based on a further approximation.

Index Terms

sparsity, generalized LASSO, duality theory

I. INTRODUCTION

The modification of quadratic optimization criteria by introducing suitable constraints leads to sparse solutions. This idea has opened new directions in many fields of signal processing, e.g., in linear regression, compressive sensing, channel identification, and equalization. The use of (possibly weighted) ℓ_1 -norms induces sparsity of the solution.

submitted to IEEE Transactions on Signal Processing on 10-Dec-2014, Manuscript ID: T-SP-18278-2014

Christoph F. Mecklenbräuer and Erich Zöchmann are with Institute of Telecommunications, Vienna University of Technology 1040 Vienna, Austria, cfm@ieee.org

Peter Gerstoft is with University of California San Diego, La Jolla, CA 92093-0238, USA <http://www.mpl.ucsd.edu/people/pgerstoft>

© IEEE 2014

The early results for sparse signals [1], [2], [3], [4] have been extended to compressible (approximately sparse) signals and sparse signals buried in noise [5], [6], [7], [8], [9] which renders the framework applicable to problems in array processing.

Tibshirani [10] noted that the generalized LASSO problem is difficult to analyze directly because the nondifferentiable ℓ_1 penalty is composed with a linear transformation. He showed that it is more intuitive to derive a solution path to the corresponding Lagrangian dual problem. Moreover, the dual approach comes without additional computational cost.

Fortunati et al. [11] found that super-resolution beyond the Rayleigh limit is achievable for compressed sensing based beamformers even for the single snapshot case. Xenaki et al. [14] noted that such techniques are implementable with single-snapshot data and irregular array configurations. Their bias and resolution analysis indicates that sparse signal reconstruction enjoys robust performance in most of the angular spectrum.

Weiss and Zoubir use an upper bound of the mean squared residuals to jointly mitigate the error contributions from noise and sensing matrix mismatch [12]. Compressed sensing can be formulated without a discrete sensing matrix, gridless compressed sensing [13], [15], [16], [17]. In this approach an atomic norm is used in the primal domain with a continuous primal variable. The support of the primal variable found in the dual domain. While more complicated, their approach have many similarities with our dual solution where we use a discrete sensing matrix and ℓ_1 norm.

Similar to [18], the generalized LASSO is formulated for complex-valued observations acquired from a sensor array. It is shown here that the corresponding dual vector is interpretable as the output of a weighted conventional beamformer (CBF) acting on the residuals of the linear observation model, cf. [19]. The maximum magnitudes of the dual vector is used for selecting the regularization parameter of the generalized LASSO. This is the basis for an efficient order-recursive procedure to solve the sparse signal reconstruction problem [20], [21], [22] at the desired sparsity level.

Further, we discuss and interpret the solutions to the generalized LASSO problem in the primal and dual domain and show its relation to the ℓ_0 -constrained solution.

A. Notation

Matrices $\mathbf{A}, \mathbf{B}, \dots$ and vectors $\mathbf{a}, \mathbf{b}, \dots$ are complex-valued and denoted by boldface letters. The zero vector is $\mathbf{0}$. The Hermitian transpose, inverse, and Moore-Penrose pseudo inverse are denoted as $\mathbf{X}^H, \mathbf{X}^{-1}, \mathbf{X}^+$ respectively. We abbreviate $\mathbf{X}^{-H} = (\mathbf{X}^H)^{-1}$. The complex vector space of dimension N is written as \mathbb{C}^N . \mathcal{N} is the null space of \mathbf{A} and $\text{span}(\mathbf{A})$ denotes the linear hull of \mathbf{A} . The projection

onto $\text{span}(\mathbf{A})$ is \mathbf{P}_A . The ℓ_p -norm is written as $\|\cdot\|_p$.

II. PROBLEM FORMULATION

We start from the following problem formulation: Let $\mathbf{y} \in \mathbb{C}^N$ and $\mathbf{A} \in \mathbb{C}^{N \times M}$. Find the best sparse solution $\mathbf{x}_{\ell_0} \in \mathbb{C}^M$ with sparsity level $s \in \mathbb{N}$ such that the squared measurement residuals are minimal,

$$\mathbf{x}_{\ell_0} = \underset{\mathbf{x}}{\operatorname{argmin}} \|\mathbf{y} - \mathbf{A}\mathbf{x}\|_2^2 \quad \text{subject to} \quad \|\mathbf{x}\|_0 \leq s, \quad (\text{P0})$$

where $\|\cdot\|_p$ denotes the ℓ_p -norm. The problem (P0) is known as ℓ_0 -reconstruction. It is *non-convex* and hard to solve, cf. [23]. Therefore, the ℓ_0 -constraint in (P0) is commonly relaxed to an ℓ_1 constraint which renders the problem (P1) to be *convex*. Further, a matrix \mathbf{D} is introduced in the formulation of the constraint which gives flexibility in the problem definition. Several variants are discussed in [10]. This gives

$$\mathbf{x}_{\ell_1} = \underset{\mathbf{x}}{\operatorname{argmin}} \|\mathbf{y} - \mathbf{A}\mathbf{x}\|_2^2 \quad \text{subject to} \quad \|\mathbf{D}\mathbf{x}\|_1 \leq \varepsilon. \quad (\text{P1})$$

In the following, this problem is referred to as the complex-valued generalized LASSO problem. Incorporating the ℓ_1 norm constraint into the objective function results in the equivalent formulation (P1'),

$$\mathbf{x}_{\ell_1} = \underset{\mathbf{x}}{\operatorname{argmin}} \left(\|\mathbf{y} - \mathbf{A}\mathbf{x}\|_2^2 + \mu \|\mathbf{D}\mathbf{x}\|_1 \right). \quad (\text{P1}')$$

The problems (P0) and (P1') yield the same sparsity level $s = \|\mathbf{x}\|_0$ of their solutions if the regularization parameter μ in (P1') is suitably chosen.

Strong duality does not hold for ℓ_0 -reconstruction (P0) and studying its dual problem does not seem a useful exercise as the duality gap is infinite. The real-valued generalized LASSO problem and its dual were analyzed in [10].

In this contribution, a similar analysis is carried out for the complex-valued problem (P1') which has straightforward applications in array signal processing. Based on this analysis, we propose and analyze an efficient procedure for approximating the solution to (P0) for a given sparsity level s which is based on the dual to (P1'). To formalize this idea, we introduce the following (non-convex) problem

$$\begin{aligned} \mathbf{x}_{\ell_1} = \underset{\mathbf{x}}{\operatorname{argmin}} & \left(\min_{\mu > 0} \left(\|\mathbf{y} - \mathbf{A}\mathbf{x}\|_2^2 + \mu \|\mathbf{D}\mathbf{x}\|_1 \right) \right) \\ & \text{subject to} \quad \|\mathbf{x}\|_0 \leq s. \end{aligned} \quad (\text{P2})$$

for which we seek an efficient solver.

III. DUAL PROBLEM TO THE GENERALIZED LASSO

The generalized LASSO problem [10] is written in constraint form, all vectors and matrices are assumed to be complex-valued. The following discussion is valid for arbitrary $N, M \in \mathbb{N}$: both the over-determined and the under-determined cases are included. Following [24], [25], a new vector $\mathbf{z} \in \mathbb{C}^M$ and a new equality constraint $\mathbf{z} = \mathbf{D}\mathbf{x}$ are introduced, to obtain the equivalent problem

$$\min_{\mathbf{x}, \mathbf{z}} (\|\mathbf{y} - \mathbf{A}\mathbf{x}\|_2^2 + \mu\|\mathbf{z}\|_1) \quad \text{subject to} \quad \mathbf{z} = \mathbf{D}\mathbf{x} . \quad (1)$$

The complex-valued dual vector $\mathbf{u} = (u_1, \dots, u_M)^T$ is introduced and associated with the new equality constraint. The corresponding Lagrangian is

$$\mathcal{L}(\mathbf{x}, \mathbf{z}, \mathbf{u}) = \|\mathbf{y} - \mathbf{A}\mathbf{x}\|_2^2 + \mu\|\mathbf{z}\|_1 + \text{Re} [\mathbf{u}^H (\mathbf{D}\mathbf{x} - \mathbf{z})] \quad (2)$$

$$= \mathcal{L}_1(\mathbf{x}, \mathbf{u}) + \mathcal{L}_2(\mathbf{z}, \mathbf{u}). \quad (3)$$

To derive the dual problem, the Lagrangian is minimized over \mathbf{x} and \mathbf{z} . The terms involving \mathbf{x} are

$$\mathcal{L}_1(\mathbf{x}, \mathbf{u}) = \|\mathbf{y} - \mathbf{A}\mathbf{x}\|_2^2 + \text{Re} (\mathbf{u}^H \mathbf{D}\mathbf{x}) . \quad (4)$$

The terms in (2) involving \mathbf{z} are

$$\mathcal{L}_2(\mathbf{z}, \mathbf{u}) = \mu\|\mathbf{z}\|_1 - \text{Re}(\mathbf{u}^H \mathbf{z}) . \quad (5)$$

The value $\hat{\mathbf{x}}$ minimizing (4) is found by differentiation. This gives

$$\mathbf{D}^H \mathbf{u} = 2\mathbf{A}^H (\mathbf{y} - \mathbf{A}\hat{\mathbf{x}}) \quad (6)$$

and

$$\mathbf{A}^H \mathbf{A}\hat{\mathbf{x}} = \mathbf{A}^H \mathbf{y} - \frac{1}{2} \mathbf{D}^H \mathbf{u} . \quad (7)$$

If $\mathbf{D}^H \mathbf{u} \in \text{span}(\mathbf{A}^H)$ the solution to (7) becomes,

$$\hat{\mathbf{x}} = \underbrace{\mathbf{A}^+ \mathbf{y} + \boldsymbol{\xi}}_{\hat{\mathbf{x}}_{\text{LS}}} - \frac{1}{2} (\mathbf{A}^H \mathbf{A})^+ \mathbf{D}^H \mathbf{u} , \quad (8)$$

where $(\cdot)^+$ denotes the Moore-Penrose pseudo inverse of \mathbf{X} , i.e. $\mathbf{X}^+ = (\mathbf{X}^H \mathbf{X})^+ \mathbf{X}^H$. Here, $\boldsymbol{\xi} \in \mathcal{N}(\mathbf{A})$ is a nullspace term which enables $\hat{\mathbf{x}}$ to deviate from the least norm solution $\mathbf{A}^+ \mathbf{y}$. The nullspace $\mathcal{N}(\mathbf{A})$ is $\{\boldsymbol{\xi} \in \mathbb{C}^M | \mathbf{A}\boldsymbol{\xi} = \mathbf{0}\}$. By identifying $\boldsymbol{\xi} = \mathbf{x}_{\ell_1}^{\text{null}}$, we specialize (8) to the solution of (P1'),

$$\mathbf{x}_{\ell_1} = \mathbf{A}^+ \mathbf{y} + \mathbf{x}_{\ell_1}^{\text{null}} - \frac{1}{2} (\mathbf{A}^H \mathbf{A})^+ \mathbf{D}^H \mathbf{u}. \quad (9)$$

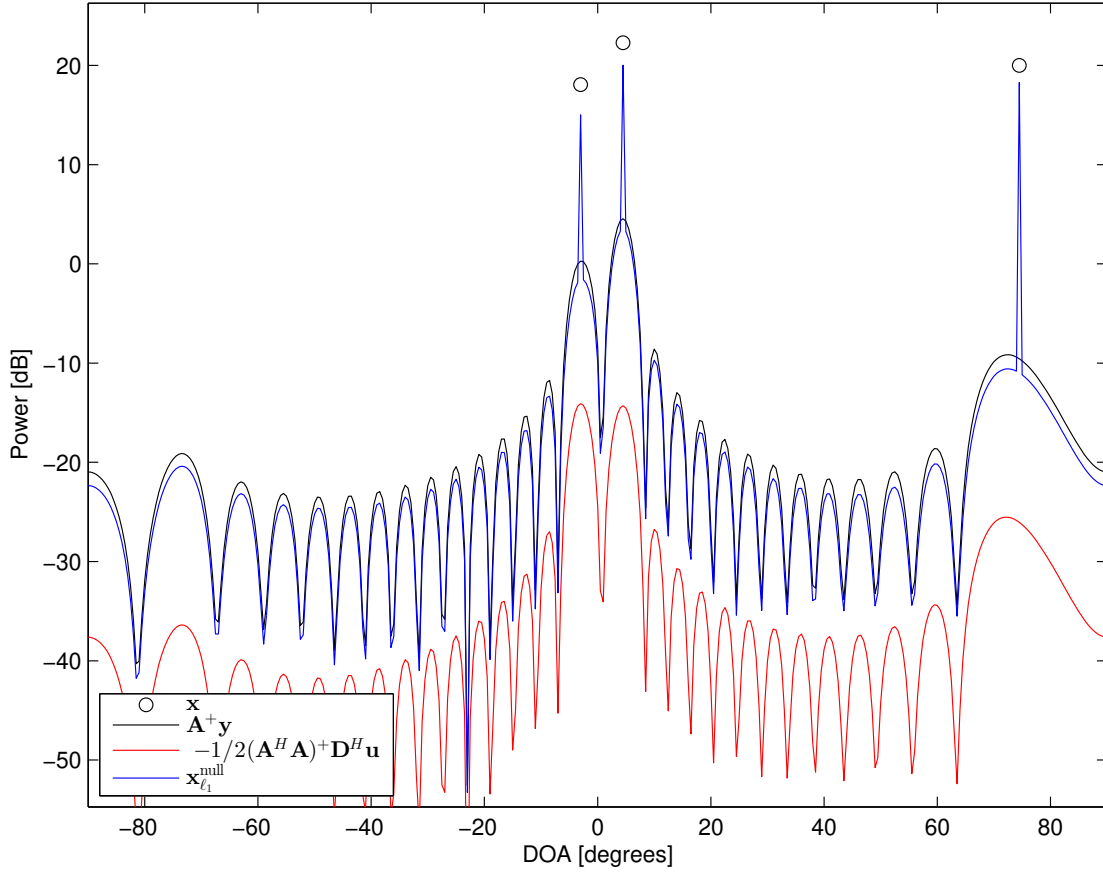


Fig. 2. Numerical example solution terms in Eq. (9) versus direction of arrival (DOA).

We evaluate (4) at the minimizing solution $\hat{\mathbf{x}}$ and express the result solely by the dual \mathbf{u} . Firstly, we expand

$$\|\mathbf{y} - \mathbf{A}\hat{\mathbf{x}}\|_2^2 = \|\mathbf{y}\|_2^2 + \|\mathbf{A}\hat{\mathbf{x}}\|_2^2 - 2 \operatorname{Re}\{\mathbf{y}^H \mathbf{A}\hat{\mathbf{x}}\} \quad (10)$$

Secondly using (6),

$$\begin{aligned} (\mathbf{D}^H \mathbf{u})^H \hat{\mathbf{x}} &= 2(\mathbf{y} - \mathbf{A}\hat{\mathbf{x}})^H \mathbf{A}\hat{\mathbf{x}} \\ &= 2\mathbf{y}^H \mathbf{A}\hat{\mathbf{x}} - 2\|\mathbf{A}\hat{\mathbf{x}}\|_2^2 \end{aligned} \quad (11)$$

Eq.(10) and the real part of (11) are summed. This results in

$$\begin{aligned} \mathcal{L}_1(\hat{\mathbf{x}}, \mathbf{u}) &= \|\mathbf{y}\|_2^2 - \|\mathbf{A}\hat{\mathbf{x}}\|_2^2 \\ &= \mathbf{y}^H \mathbf{y} - \|\tilde{\mathbf{y}} - \tilde{\mathbf{D}}^H \mathbf{u}\|_2^2, \end{aligned} \quad (12)$$

where we used (8) and introduced the abbreviations

$$\tilde{\mathbf{D}} = \frac{1}{2}\mathbf{D}\mathbf{A}^+, \quad (13)$$

$$\mathbf{A}\mathbf{A}^+ = \mathbf{P}_A, \quad (14)$$

$$\tilde{\mathbf{y}} = \mathbf{P}_A \mathbf{y}. \quad (15)$$

Formally, the subspace constraint $\mathbf{D}^H \mathbf{u} \in \text{span}(\mathbf{A}^H)$ is formulated as $(\mathbf{D}\mathbf{U})^H \mathbf{u} = \mathbf{0}$ where \mathbf{U} is a unitary basis of the null space \mathcal{N} . This results in

$$\inf_{\mathbf{x}} \mathcal{L}_1(\mathbf{x}, \mathbf{u}) = \begin{cases} \mathbf{y}^H \mathbf{y} - \|\tilde{\mathbf{y}} - \tilde{\mathbf{D}}^H \mathbf{u}\|_2^2, & \text{if } (\mathbf{D}\mathbf{U})^H \mathbf{u} = \mathbf{0}, \\ -\infty, & \text{otherwise.} \end{cases} \quad (16)$$

Next (5) is minimized with respect to \mathbf{z} , see Appendix A,

$$\inf_{\mathbf{z}} \mathcal{L}_2(\mathbf{z}, \mathbf{u}) = \begin{cases} 0, & \text{if } \|\mathbf{u}\|_\infty \leq \mu \\ -\infty, & \text{otherwise.} \end{cases} \quad (17)$$

Combining (16) and (17), the dual problem to the generalized LASSO (1) is,

$$\max_{\mathbf{u} \in \mathbb{C}^M} \mathbf{y}^H \mathbf{y} - \|\tilde{\mathbf{y}} - \tilde{\mathbf{D}}^H \mathbf{u}\|_2^2 \quad (18a)$$

$$\text{subject to} \quad \|\mathbf{u}\|_\infty \leq \mu, \quad (18b)$$

$$(\mathbf{D}\mathbf{U})^H \mathbf{u} = \mathbf{0}. \quad (18c)$$

Equation (6) can be solved for \mathbf{u} if the row space constraint (18c) is fulfilled. The result is summarized in the following

Theorem 1. *If \mathbf{D} is non-singular, the dual vector \mathbf{u} is the output of a weighted CBF acting on the vector of residuals, i.e.*

$$\mathbf{u} = 2\mathbf{D}^{-H} \mathbf{A}^H (\mathbf{y} - \mathbf{A}\mathbf{x}_{\ell_1}), \quad (19)$$

where \mathbf{x}_{ℓ_1} is such that the box constraint (18b) is fulfilled.

The dual vector \mathbf{u} gives an indication of the sensitivity of the primal solution to small changes in the constraints of the primal problem [24]. In [10], it was worked out for the real-valued case that the solution to (P1') can be more easily constructed and better understood via the dual problem. Theorem 1 asserts a linear one-to-one relation between the corresponding dual and primal solution vectors also in the complex-valued case. Thus, any results formulated in the primal domain are readily applicable in the dual domain. This allows a more fundamental interpretation of sequential Bayesian approaches to density evolution for sparse source reconstruction [20], [21]: they can be rewritten in a form that shows that they

solve a generalized complex-valued LASSO problem and its dual. The posterior probability density is actually related to the dual solution.

The following corollaries clarify useful element-wise relations between the primal and dual solutions: Corollary 1 relates the *magnitudes* of the corresponding primal and dual coordinates. Further, Corollary 2 certifies what conditions on \mathbf{D} are sufficient for guaranteeing that the *phase angles* of the corresponding primal and dual coordinates are equal. Finally, Corollary 3 states that *both* the primal and the dual solutions to (P1') are piecewise linear in the regularization parameter μ .

Corollary 1. *If the m th primal coordinate is active, i.e. $x_{\ell_1, m} \neq 0$ then the box constraint (18b) is tight in the m th dual coordinate. Formally,*

$$x_{\ell_1, m} \neq 0 \quad \Rightarrow \quad |u_m| = \mu, \quad (m = 1, \dots, M). \quad (20)$$

Informally, we say that the m th dual coordinate hits the boundary when the m th primal coordinate becomes active. Conversely, when the bound on $|u_m|$ is loose (i.e. the constraint on u_m is inactive), the corresponding primal variable x_m is zero (the m th primal coordinate is inactive). The proof is given in Appendix B. The active set \mathcal{M} is

$$\mathcal{M} = \{m \mid x_{\ell_1, m} \neq 0\} \subseteq \{m \mid |u_m| = \mu\} = \mathcal{U}. \quad (21)$$

The active set \mathcal{M} implicitly depends on the choice of μ in problem (P1'). Let \mathcal{M} contain exactly s indices,

$$\mathcal{M} = \{m_1, m_2, \dots, m_s\}. \quad (22)$$

Corollary 2. *If matrix \mathbf{D} is diagonal with real-valued positive diagonal entries, then the phase angles of the corresponding entries of the dual and primal solution vectors are equal.*

$$\arg(u_m) = \arg(x_{\ell_1, m}), \quad \forall m \in \mathcal{M} \quad (23)$$

Corollary 3. *The primal and the dual solutions to the complex-valued generalized LASSO problem (P1') are continuous and piecewise linear in the regularization parameter $\mu > 0$. The changes in slope occur at those values for μ where the set of active indices \mathcal{M} changes.*

The proofs for these corollaries are given in Appendix B.

A. Relation to the ℓ_0 solution

It is now assumed that \mathcal{M} defines the indices of the s non-zero elements of the corresponding ℓ_0 solution. In other words: the ℓ_1 and ℓ_0 solutions share the same sparsity pattern. The ℓ_0 solution with

sparsity s is then obtained by regressing the s *active* columns of \mathbf{A} to the data \mathbf{y} in the least-squares sense. Let

$$\mathbf{A}_{\mathcal{M}} = [\mathbf{a}_{m_1}, \mathbf{a}_{m_2}, \dots, \mathbf{a}_{m_s}] , \quad (24)$$

where \mathbf{a}_m denotes the m th column of \mathbf{A} . The ℓ_0 solution becomes (cf. Appendix C)

$$\mathbf{x}_{\ell_0} = \mathbf{A}_{\mathcal{M}}^+ \mathbf{y} . \quad (25)$$

Here, $\mathbf{A}_{\mathcal{M}}^+ = (\mathbf{A}_{\mathcal{M}}^H \mathbf{A}_{\mathcal{M}})^{-1} \mathbf{A}_{\mathcal{M}}^H$ is the left inverse of $\mathbf{A}_{\mathcal{M}}$. By subtracting (9) from (25) and restricting the equations to the contracted basis $\mathbf{A}_{\mathcal{M}}$ yields

$$\mathbf{A}_{\mathcal{M}}(\mathbf{x}_{\ell_0} - \mathbf{x}_{\ell_1}) = \frac{1}{2} \mathbf{A}_{\mathcal{M}} (\mathbf{A}_{\mathcal{M}}^H \mathbf{A}_{\mathcal{M}})^+ \mathbf{D}_{\mathcal{M}}^H \mathbf{u}_{\mathcal{M}} \quad (26)$$

$$= \tilde{\mathbf{D}}_{\mathcal{M}}^H \mu e^{j\theta} . \quad (27)$$

In the image of \mathbf{A} , the ℓ_0 -reconstruction problem (P0) and the generalized LASSO (P1') coincide if the LASSO problem is pre-informed (prior knowledge) by setting \mathbf{D}_{mm} , $m \in \mathcal{M}$ to zero. The prior knowledge is obtainable by an iterative re-weighting process [26] or by a sequential procedure on stationary sources [21].

IV. DIRECTION OF ARRIVAL ESTIMATION

For the numerical examples, we model a uniform linear array (ULA), which is described with its steering vectors representing the incident wave for each array element.

A. Array Data Model

Let $\mathbf{x} = (x_1, \dots, x_M)^T$ be a vector of complex-valued source amplitudes. We observe time-sampled waveforms on an array of N sensors which are stacked in the vector \mathbf{y} . The following linear model for the narrowband sensor array data \mathbf{y} at frequency ω is assumed,

$$\mathbf{y} = \mathbf{A}\mathbf{x} + \mathbf{n} . \quad (28)$$

The m th column of the transfer matrix \mathbf{A} is the array steering vector \mathbf{a}_m for hypothetical waves from direction of arrival (DOA) θ_m . To simplify the analysis all columns are normalized such that their ℓ_2 norm is one. The transfer matrix \mathbf{A} is constructed by sampling all possible directions or arrival, but only very few of these correspond to real sources. Therefore, the dimension of \mathbf{A} is $N \times M$ with $N \ll M$ and \mathbf{x} is sparse. In our setting, the number of hypothetical source locations M is much larger than the number of sensors N , i.e. $N \ll M$. The linear model equations (28) are underdetermined.

The nm th element of \mathbf{A} is modeled by

$$A_{nm} = \frac{1}{\sqrt{N}} \exp [j(n-1)\pi \sin \theta_m]. \quad (29)$$

Here $\theta_m = \frac{\pi(m-1)}{M} - \pi/2$ is the DOA of the m th hypothetical DOA to the n th array element.

The additive noise vector \mathbf{n} is assumed spatially uncorrelated and follows a zero-mean complex normal distribution with diagonal covariance matrix $\sigma^2 \mathbf{I}$.

For the observation \mathbf{y} according to the linear model (28), the conditional probability density given the source vector \mathbf{x} is

$$p(\mathbf{y}|\mathbf{x}) = \frac{\exp\left(-\frac{1}{\sigma^2}\|\mathbf{y} - \mathbf{A}\mathbf{x}\|_2^2\right)}{(\pi\sigma^2)^N}. \quad (30)$$

For the source vector \mathbf{x} , a prior probability density is assumed in form of a multivariate complex Laplace-like density [27],

$$p(\mathbf{x}) = \prod_{m=1}^M \left(\frac{\lambda_m}{\sqrt{2\pi}}\right)^2 e^{-\lambda_m|x_m|}, \quad (31)$$

with associated hyperparameters $\lambda_m > 0$ modeling the source signal strength at location θ_m . $x_m = |x_m|e^{j\phi_m}$ is the complex source signal at hypothetical source location θ_m . Note that (31) defines a joint distribution for $|x_m|$ and ϕ_m for all $m = 1, \dots, M$. Taking the logarithm gives

$$-\ln p(\mathbf{x}) = \sum_{m=1}^M \lambda_m|x_m| - 2 \sum_{m=1}^M \ln \lambda_m + M \ln 2\pi. \quad (32)$$

For the posterior probability density function (pdf) $p(\mathbf{x}|\mathbf{y})$, Bayes' rule is used for obtaining the generalized LASSO Lagrangian [10], [21]

$$\frac{1}{\sigma^2}\|\mathbf{y} - \mathbf{A}\mathbf{x}\|_2^2 + \mu \|\mathbf{W}\mathbf{x}\|_1 \quad (33)$$

with

$$\mathbf{W} = \frac{1}{\mu} \text{diag}(\boldsymbol{\lambda}) = \text{diag}(\mathbf{w}). \quad (34)$$

Minimizing the generalized LASSO Lagrangian (35) with respect to \mathbf{x} for given μ , and $\mathbf{w} = (w_1, \dots, w_M)^T$, $\boldsymbol{\lambda} = \mu\mathbf{w}$, gives a sparse MAP source estimate \mathbf{x}_{ℓ_1} . This minimization problem promotes sparse solutions in which the ℓ_1 constraint is weighted by giving every source amplitude its own hyperparameter w_m .

Equivalently to (33), this is reformulated as

$$\|\mathbf{y} - \mathbf{A}\mathbf{x}\|_2^2 + \mu \|\mathbf{D}\mathbf{x}\|_1, \quad (35)$$

with

$$\mathbf{D} = \sigma^2 \mathbf{W}. \quad (36)$$

The minimization of (35) constitutes a strictly convex optimization problem.

B. Basis coherence

The chosen examples feature different levels of basis coherence in order to examine the solution's behavior. As described in [14], the *basis coherence* is a measure of correlation between two steering vectors and defined as the inner product between atoms, i.e. the columns of \mathbf{A} . The maximum of these inner products is called mutual coherence and is customarily used for performance guarantees of recovery algorithms. To state the difference formally:

$$\text{coh}(\mathbf{a}_i, \mathbf{a}_j) = \mathbf{a}_i^H \mathbf{a}_j \quad (37)$$

$$\text{mutual coh}(\mathbf{A}) = \|\mathbf{A}^H \mathbf{A} - \mathbf{I}\|_\infty \quad (38)$$

The mutual coherence is bounded between 0 and 1 and [14] has shown that the coherence defines a region of possible offsets around the true DOA θ_m associated with steering vector \mathbf{a}_m . The region of possible offsets is marked in Fig. 7 as circles (“o”).

C. Numerical Example

The following numerical example in Figs. 3 and 4 demonstrates the dual solution and the classical CBF output for $N = 30$ and $M = 361$. The example is noiseless and the diagonal matrix $\mathbf{D} = \mathbf{I}$ is non-informative in the Bayesian sense. In Fig. 3, the LASSO with $\mu = 1$ is solved for a scenario with three sources at DOA $-5^\circ, 10^\circ, 150^\circ$ and all sources have same power level (see Fig. 3b), whereas in Fig. 4, an additional fourth source at 14° is included into the scenario.

1) *CBF resolvable regime:* In Fig. 3, we investigate the performance when the steering vectors of the active sources have small basis coherence. The basis of source 1 is weakly coherent with source 2, $\text{coh} \approx 0.02$ using (37).

Figure 3a shows the normalized beampattern of the CBF (blue) and the pattern of the dual vector (black). This figure shows that the true source parameters (DOA and power) are well estimated.

2) *Beyond the CBF capabilities:* Figure 4a shows that the sources are not separable with the CBF, because the steering vectors belonging to source 2 and 3 are coherent, $\text{coh} = 0.61$ using (37). The (generalized) LASSO approach is still capable of resolving all 4 sources. Figure 4b shows that the true source locations (DOA) are still well estimated, in contrast to the source powers.

V. SOLUTION PATH

The problems (P0)–(P2) are complex-valued and the corresponding solution paths behave differently from what is described in Ref. [10]. In the following figures, only the magnitudes of the primal and dual

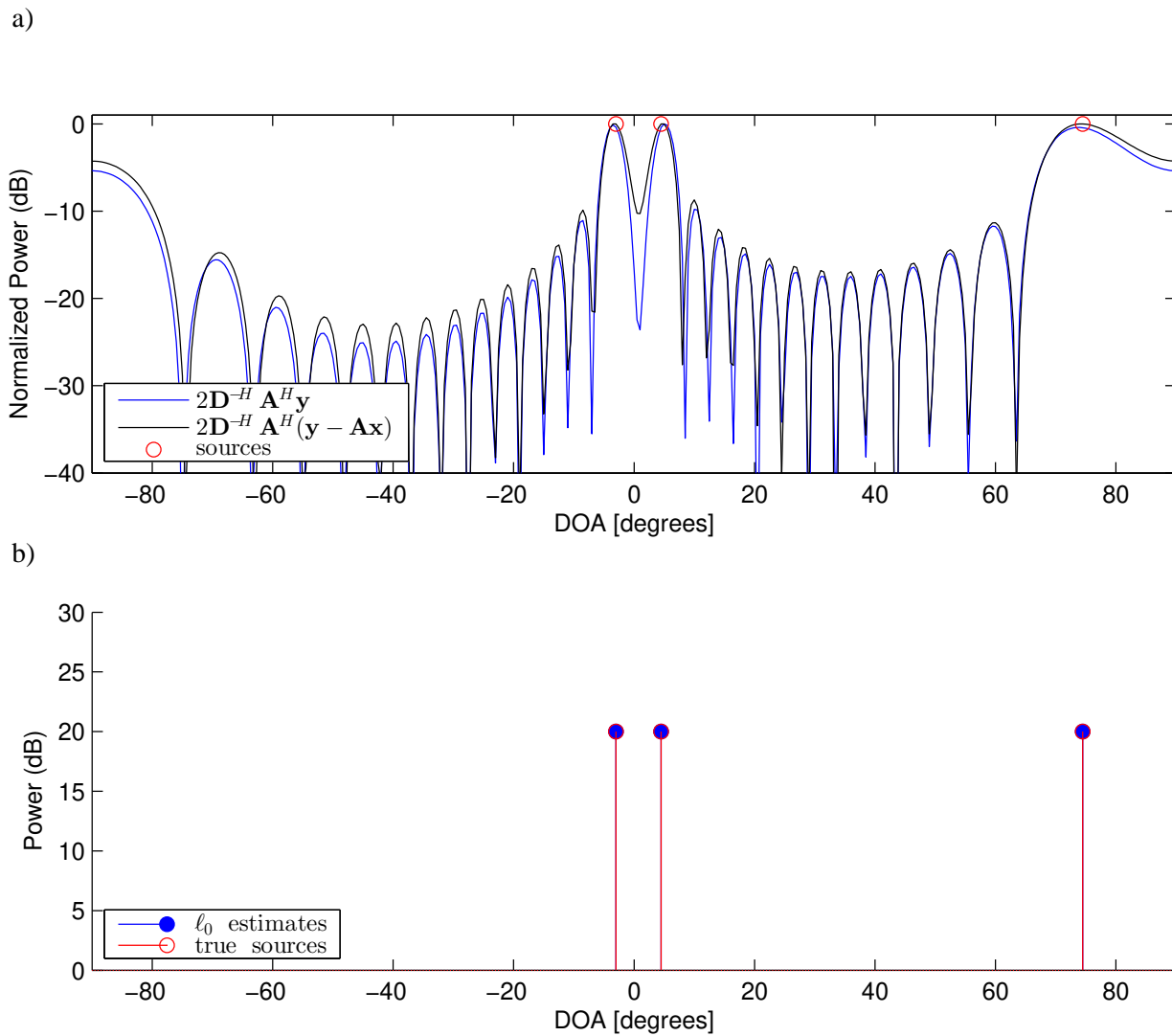


Fig. 3. Dual (a) and primal (b) coordinates for 3 well separated sources with low basis coherence.

solution coordinates are illustrated. Note that Corollary 1 guarantees that the phases of the active primary solution elements and their duals are identical and independent from μ .

A. Complete Basis

First (Fig. 5) discusses the dual and primal solution for a complete basis with $M = 6$, sparsity level $s = 6$, and $N = 30$ sensors linearly spaced with half wavelength spacing. This simulation scenario is not sparse and all steering vectors \mathbf{a}_m for $1 \leq m \leq M$ will eventually be used to reconstruct the data for

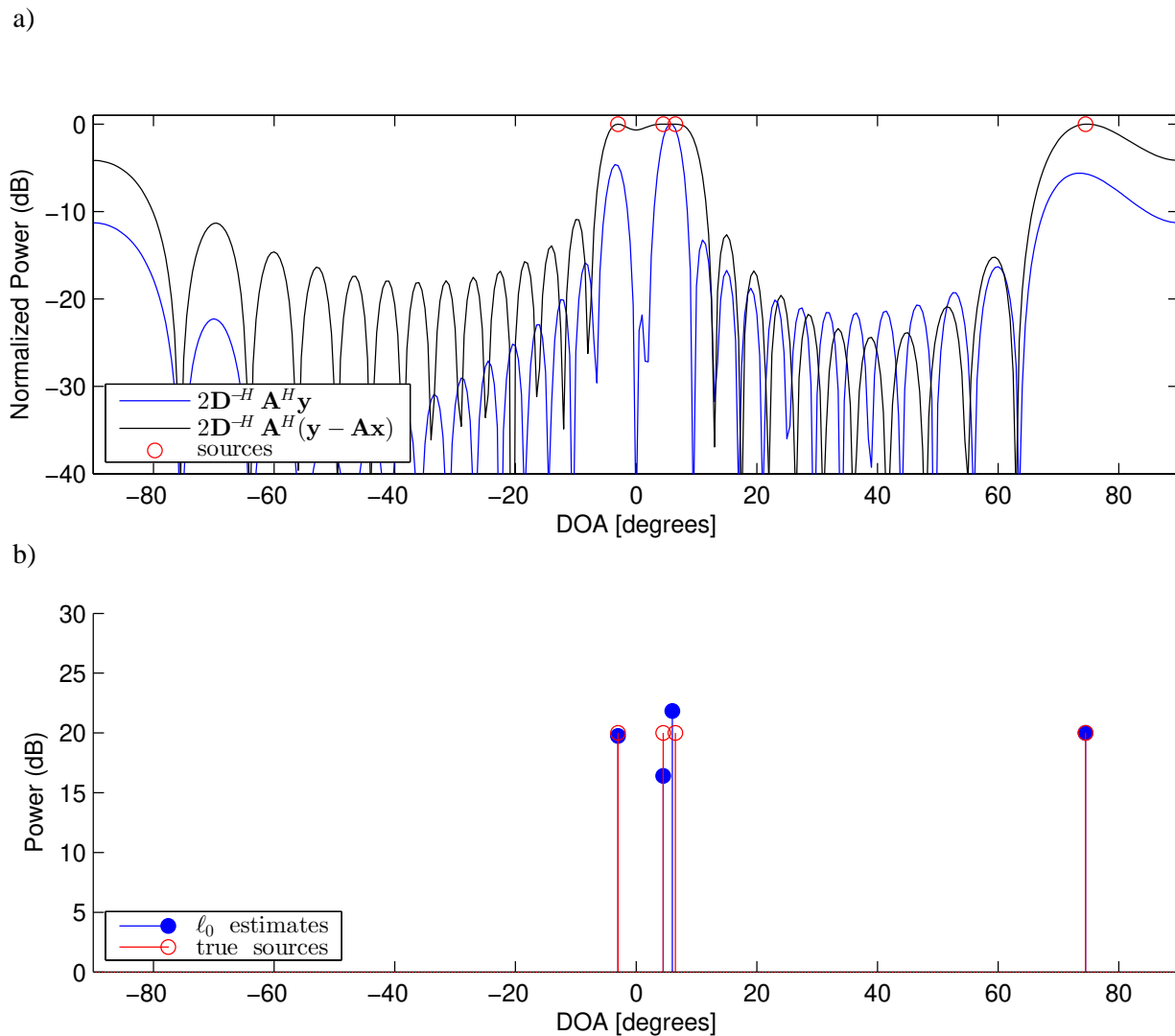


Fig. 4. Dual (a) and primal (b) coordinates for 4 sources with higher basis coherence.

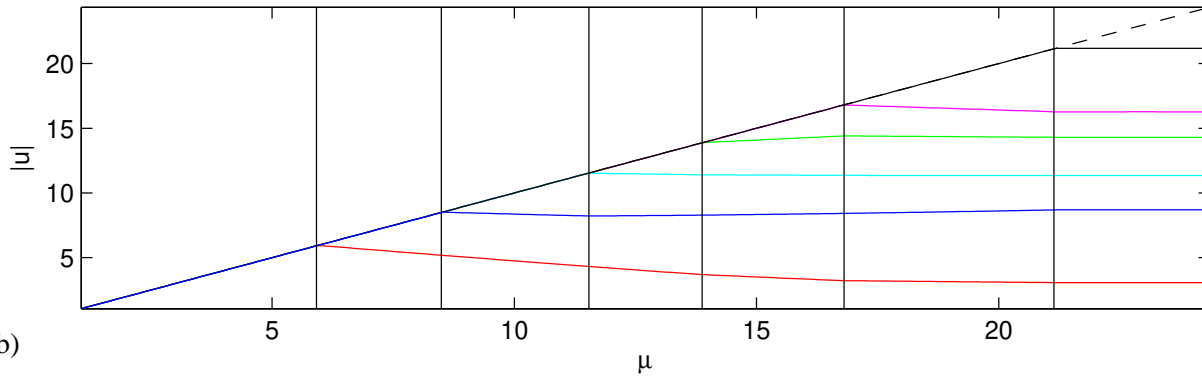
small μ . The source parameters that are used in the simulation scenario are given in Table I. The signal to noise ratio is defined as

$$\text{SNR} = 10 \log_{10} \left(\mathbb{E} \|\mathbf{Ax}\|_2^2 / \mathbb{E} \|\mathbf{n}\|_2^2 \right) \text{ dB}, \quad (39)$$

and chosen to be $\text{SNR} = 40$ dB. The diagonal matrix $\mathbf{D} = \mathbf{I}$ is again chosen to be non informative.

We discuss the solution paths in Figs. 5–9 from right ($\mu = \infty$) to left ($\mu = 0$). Initially all dual solution paths are horizontal (slope = 0), since the primal solution $\mathbf{x}_{\ell_1} = \mathbf{0}$ for $\mu > 2\|\mathbf{D}^{-H}\mathbf{A}^H\mathbf{y}\|_\infty$. In this strongly penalized regime, the dual vector is the output of the weighted CBF $\mathbf{u} = \mathbf{D}^{-H}\mathbf{A}^H\mathbf{y}$ which

a)



b)

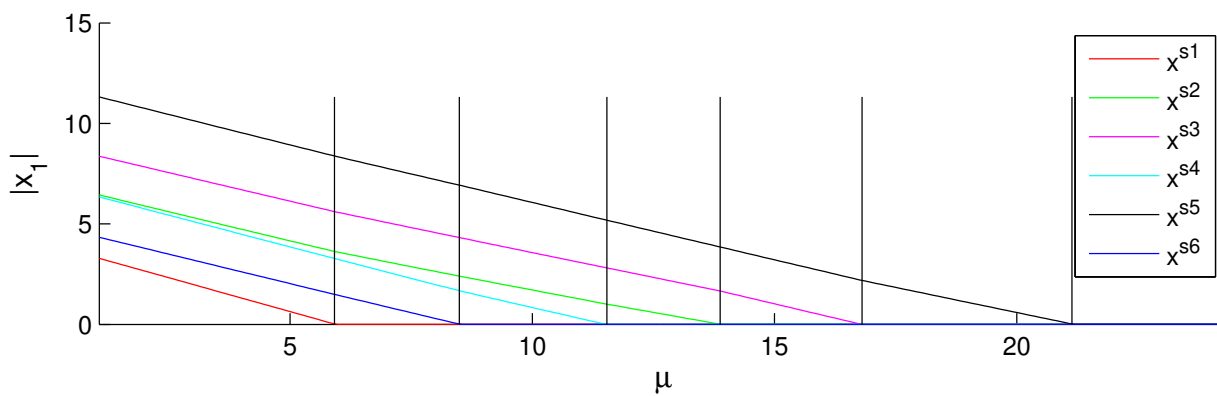


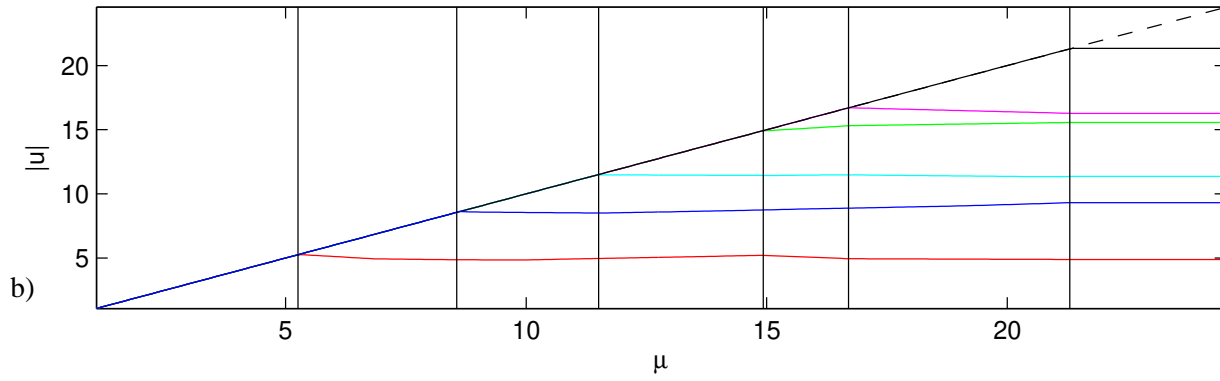
Fig. 5. Magnitudes of the solution paths versus μ for the simulation parameters in Table I and SNR = 40 dB: (a) dual, and (b) primal vectors for the case of the *complete basis*.

No.	DOA ($^{\circ}$)	Power (lin.)
1	-6.0	4.0
2	-1.0	7.0
3	4.0	9.0
4	9.0	7.0
5	14.0	12.0
6	19.0	5.0

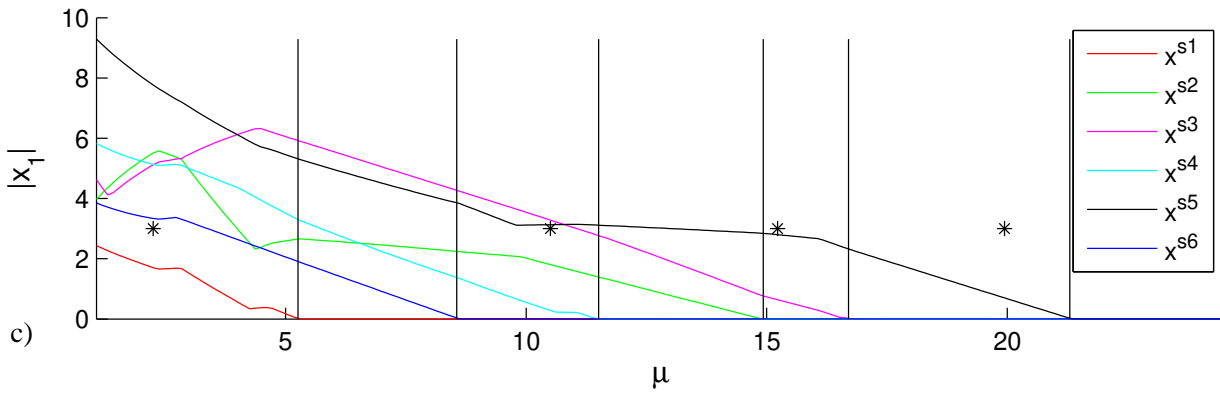
TABLE I

SOURCE PARAMETERS FOR SIMULATION SCENARIO

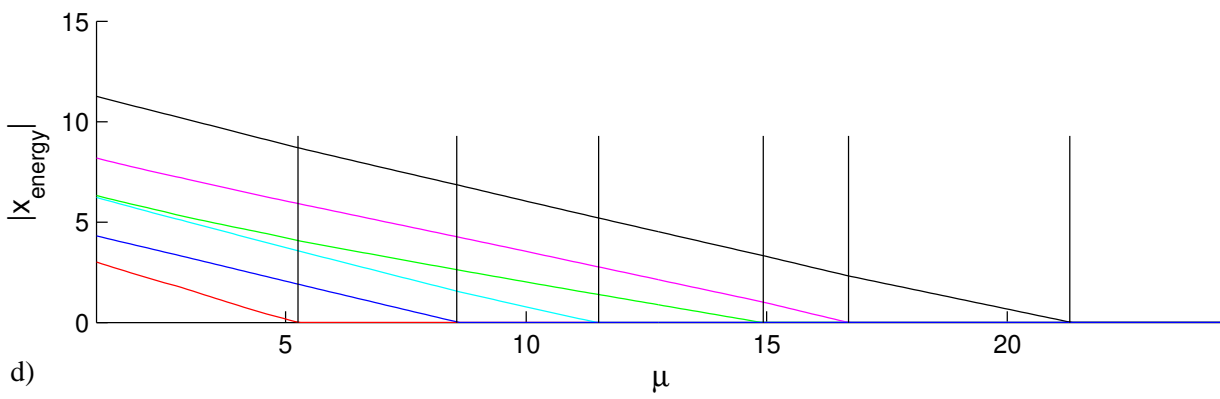
a)



b)



c)



d)

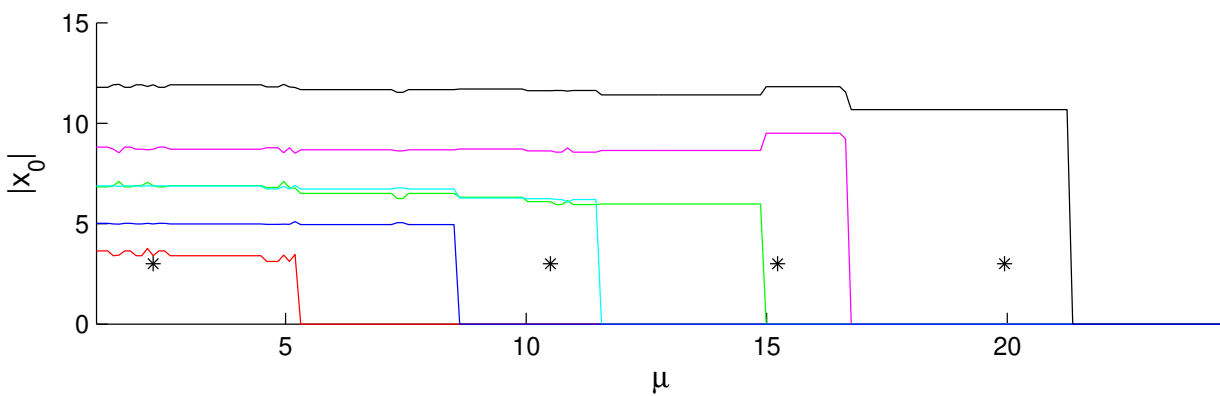


Fig. 6. Magnitudes of the solution paths versus μ for the simulation parameters in Table I and SNR = 40 dB: (a) dual, and

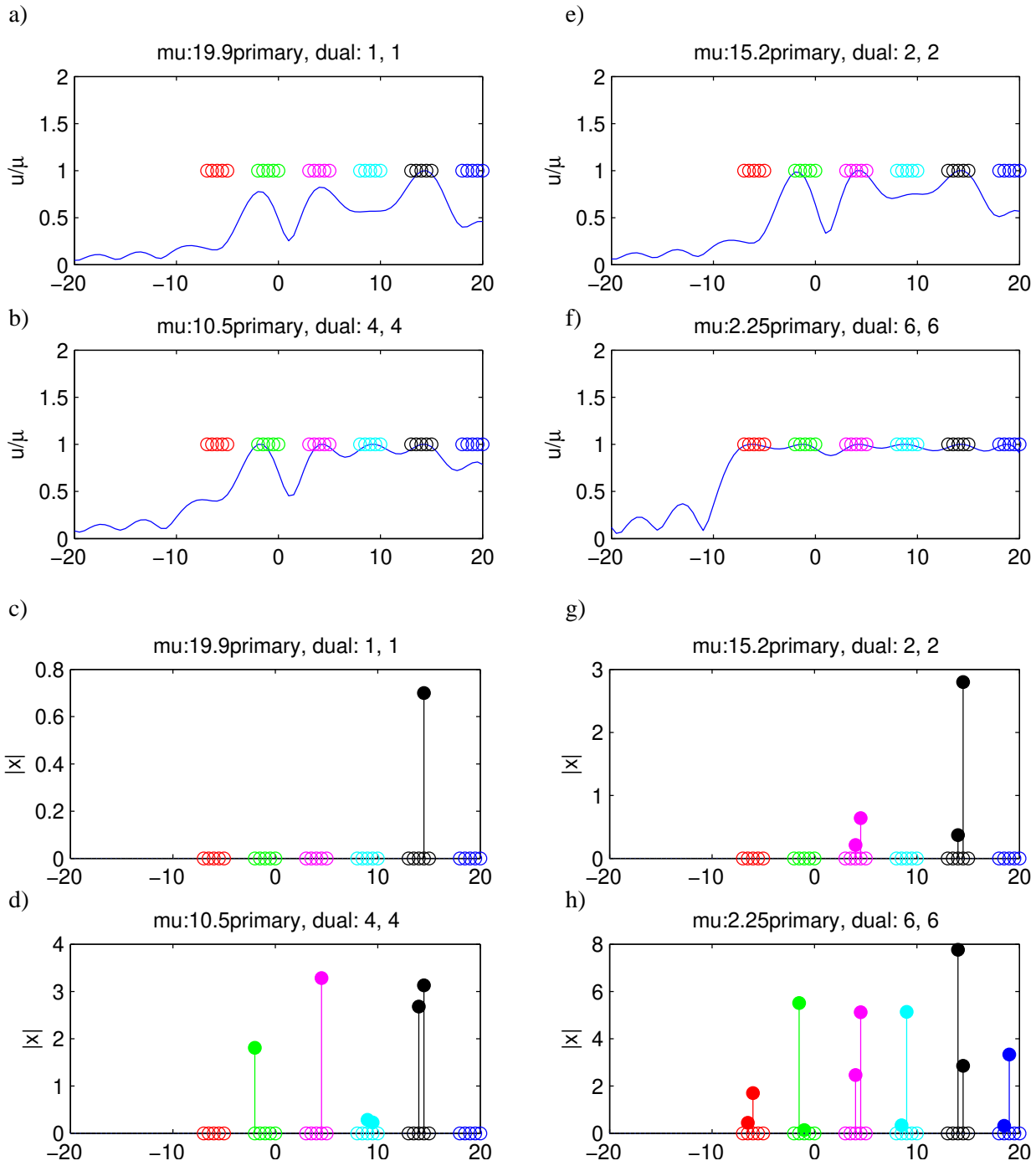


Fig. 7. Dual and primal coordinates at selected values of μ for 81-vector overcomplete basis for SNR = 40 dB.

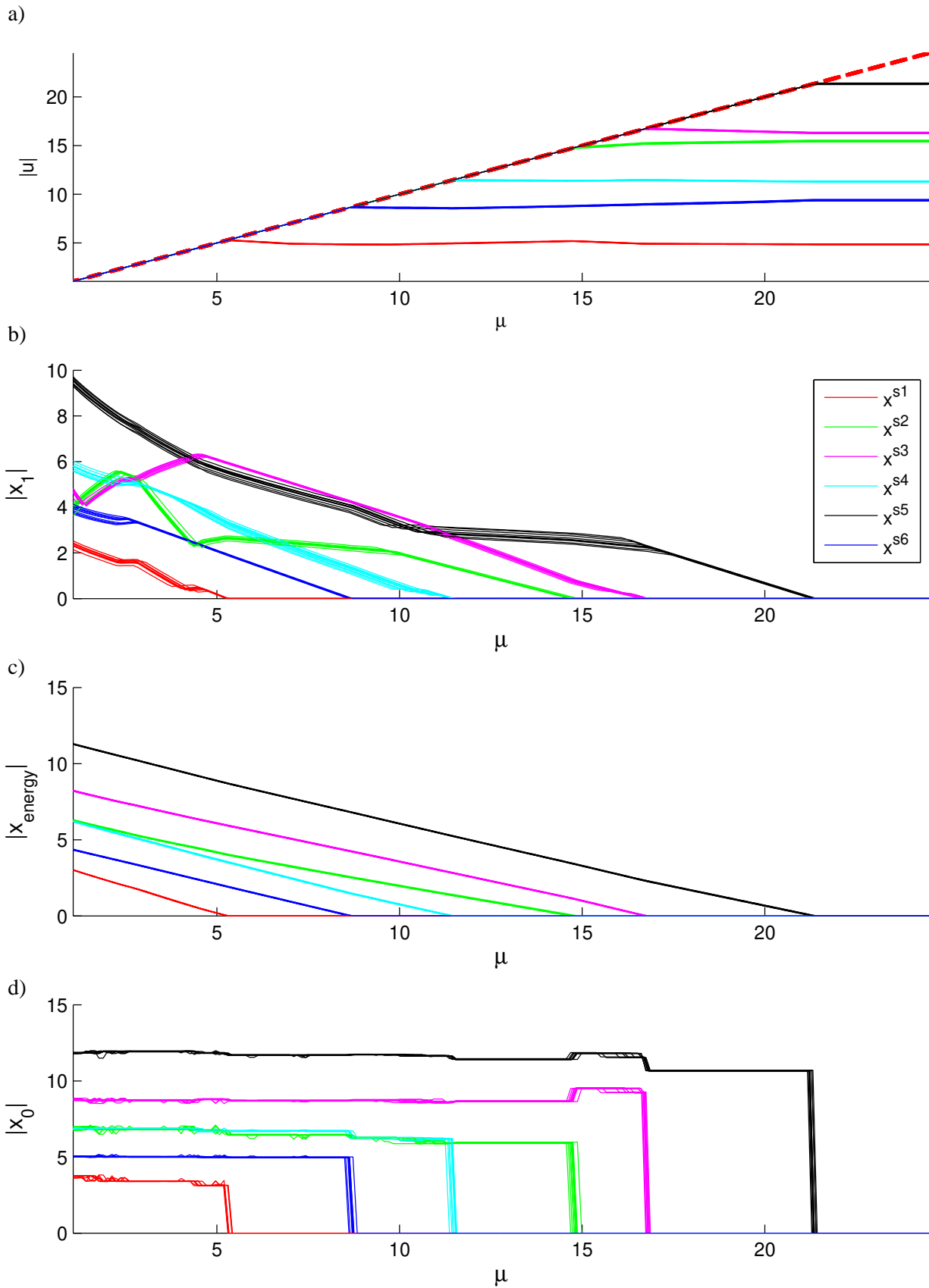


Fig. 8. For 10 noise realizations, magnitudes of the solution paths versus μ for the simulation parameters in Table I and

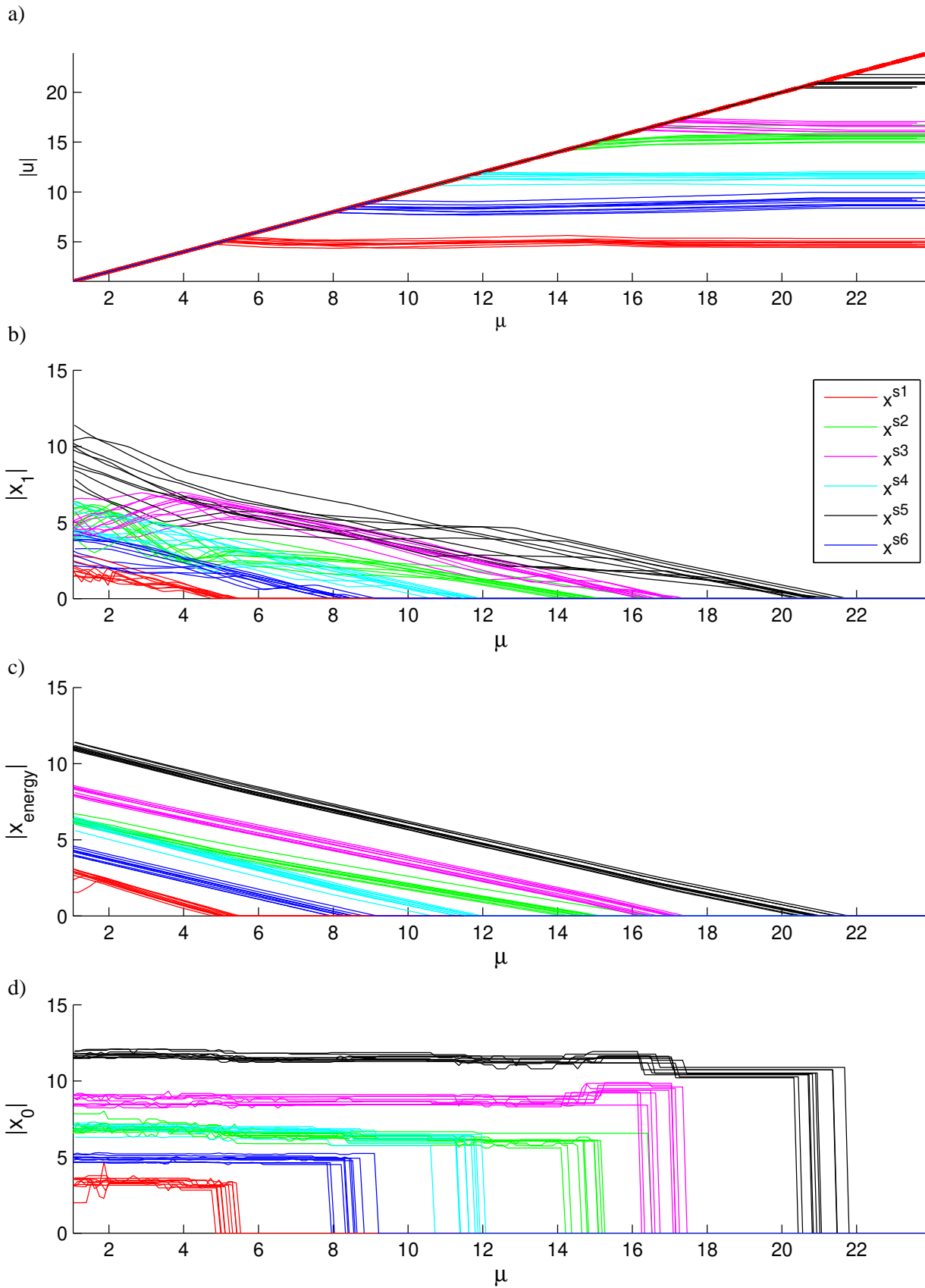


Fig. 9. As Fig. 8, but with SNR = 20 dB:

does not depend on μ .

At the point $\mu^1 = 2\|\mathbf{D}^{-H}\mathbf{A}^H\mathbf{y}\|_\infty$ the first dual coordinate hits the boundary (18b). This occurs at $\mu^1 = 21$ in Fig. 5a and the corresponding primal coordinate becomes active. As long the active set \mathcal{M} does not change, the magnitude of the corresponding dual coordinate is μ , due to Corollary 1. The remaining dual coordinates change slope relative to the basis coherence level of the active set.

As μ decreases, the source magnitudes at the primal active indices increase since the ℓ_1 -constraint in (P1') becomes less important, see Fig. 5b. The second source will become active when the next dual coordinate hits the boundary (at $\mu^1 = 17$ in Fig. 5).

When the active set is constant, the primary and dual solution is piecewise linearly with μ , as proved in Corollary 3. The changes in slope are quite gentle, as shown for the example in Fig. 5. Finally, at $\mu = 0$ the problem (P1') degenerates to an unconstrained (underdetermined) least squares problem. Its primal solution $\hat{\mathbf{x}} = \hat{\mathbf{x}}_{\text{LS}}$, see (8), is not unique and the dual vector is trivial, $\mathbf{u} = \mathbf{0}$.

B. Overcomplete Basis

We now enlarge the basis to $M = 81$ with hypothetical source locations $\theta_m \in [-20^\circ, 20^\circ]$ with 0.5° spacing, and all other parameters as before. The solution is now sparse.

The LASSO path [28] is illustrated in Fig. 6 where we expect the source location estimate to be up to ± 2 bins from the true source location. The dual Fig. 6a appears to be quite similar to Fig. 5a.

Corollary 3 gives that the primary solution should change linearly, as demonstrated for the complete basis in Fig. 5b). Here we explain why this is not the case for the overcomplete basis primary solution in Fig. 6b. This can be understood by examining the full solution at selected values of μ (stars (*) in Fig. 6). At $\mu = 20$ just one solution is active, only the black source (source 5) is active though one bin to the left, as shown in Fig. 7. Between $\mu = 16$ and $\mu = 11$, the black source appears constant, this is because at large values the source is initially located in a neighboring bin. As μ decreases, the correct bin receive more power, see Fig7 for $\mu = 15$ and $\mu = 10$. When it is stronger than the neighbor bin at ($\mu = 11$), this source power will start increase again. This trading in source power causes the fluctuations in Fig. 6b.

One way to correct for this fluctuation is to sum the coherent energy for all bins near a source, i.e., multiplying the source vector with the corresponding neighbor columns of \mathbf{A} and then compute the energy based on the average received power at each sensor. This gives a steady rise in power as shown in Fig. 6c.

We motivate solving (P1') as a substitute for ℓ_0 -reconstruction (P0)—finding the active indexes of the ℓ_1 solution, see Fig. 6d. The ℓ_0 primal can be found with the restricted basis and the value of the ℓ_1 primal from (8), which depends on μ , or by just solving (25).

To investigate the sensitivity to noise, 10 LASSO paths are simulated for 10 noise realizations for both SNR = 40 dB (Fig. 8) and SNR = 20 dB (Fig 9). The dual (Figs. 8a and 9a), appears quite stable to noise, but the primal $|\mathbf{x}_{\ell_1}|$ (Figs. 8b and 9b) show quite large variation with noise. This is because the noise causes the active indexes to shift and thus the magnitude to vary. The mapping to energy $|\mathbf{x}_{\text{energy}}|$ (Figs. 8c and 9c) or the $|\mathbf{x}_{\ell_0}|$ solution (Figs. 8d and 9d) makes the solution much more stable.

VI. SOLUTION PROCEDURES

Motivated by Theorem 1 and Corollary 1, we propose the order-recursive procedure in Table II for approximating the solution to problem (P2), a faster iterative procedure in Table III, and a dual-based iterative procedure in Table IV.

As shown by Theorem 1, the dual vector is actually a CBF acting on the LASSO residuals which will hit the boundary ($|u_m| = \mu$) if the corresponding primal coordinate x_m is active. This insight leads to an estimator for the regularization parameter μ for a given sparsity order.

The LASSO path [28] is illustrated in Fig. 10. Starting from a large choice of regularization parameter μ and then decreasing, we observe incremental changes in the active set at specific values μ^{*p} of the regularization parameter. The active set remains constant within the interval $\mu^{*p} > \mu > \mu^{*(p+1)}$. Assuming the sequence $\mu^{*1}, \mu^{*2}, \dots$ known, we follow a path of regularization parameters μ^1, μ^2, \dots where μ^p is slightly higher than the lower end $\mu^{*(p+1)}$ of the regularization interval. Specifically, $\mu^p = (1 - F)\mu^{*p} + F\mu^{*(p+1)}$ with $F < 1$. For the numerical examples $F = 0.9$ is used. This F is chosen because the primal solution \mathbf{x}_{ℓ_1} is closest to \mathbf{x}_{ℓ_0} at the lower end of the interval.

The order recursive procedure in Table II finds one source at a time as μ is lowered, the iterative procedure in Table III iterates on the finding the number of active sources, the dual iterative procedure in Table IV is entirely in the dual domain. In the following we focus on the 1 order recursive procedure, and indicate the differences to the other approaches.

A. Primary-based

The procedure starts with the all-zero solution $\mathbf{x}_{\ell_1}^0 = \mathbf{0}$ in line 1. This corresponds to a large value of $\mu = \mu^0 > 2\|\mathbf{D}^{-H}\mathbf{A}^H\mathbf{y}\|_\infty$, but is not used directly. The first value of μ , μ^1 is chosen based on the first peak in \mathbf{u} for $\mathbf{x}_{\ell_1} = \mathbf{0}$. The ℓ_∞ -norm is implemented by calling the $\text{peak}(\mathbf{u}, p)$ -function for $p = 1$

in line 3. For this purpose, we define the $\text{peak}(\mathbf{u}, p)$ -function which returns the p th largest local peak in magnitude of the vector \mathbf{u} . A local peak is defined as an element which is larger than its adjacent elements.

In lines 4–5 in Table II, the generalized LASSO problem (P1') is solved for $\mu = \mu^1$ and the corresponding active set is detected by thresholding (at this point, the active set contains only a single active index). Then, by assuming that the active set is also valid for the solution to the ℓ_0 -problem (P0), the solution $\mathbf{x}_{\ell_0}^p$ is computed. Next, we start an iteration loop with counter i which reduces the regularization parameter μ by inserting the updated dual variable \mathbf{u}_1 into line 3.

The next choice of regularization parameter μ^2 is selected in the interval $[\mu^{*2}, \mu^{*3}[$ which we estimate by the 2nd and 3rd largest peaks of the dual variable. This is illustrated in Fig. 10. This is implemented in line 3. Then, we solve (P1') for $\mu = \mu^2 < \mu^1$ and continue the iteration until the desired sparsity level s is reached.

In line 5, the active set \mathcal{M} is approximated by thresholding of the primal solution.

If the number of elements in \mathcal{M} equals the loop counter i then the basis is restricted to \mathcal{M} and the corresponding ℓ_0 -solution is computed in lines 9–13. Otherwise, at least one peak of the dual vector is a sidelobe artifact. Then an *additional* peak in \mathbf{u} must be included for estimating the next μ . This is implemented by incrementing the loop counter i in line 8, which keeps track of the number of peaks in \mathbf{u} .

The order-recursive procedure in Table II employs an approximation of the height of the i th local peak given the $(i-1)$ th solution. Theorem 1 together with Corollary 1 gives $\mu^i = \text{peak}(\mathbf{u}^i, i)$. The underlying assumption is that the next source will become active at the location corresponding to the dual coordinate of the next peak. This assumption is not universally valid as discussed below (44).

From the box constraint (18b), it is concluded that the level of the i th peak in \mathbf{u} does not change much during the iteration over i : It is bounded by the difference in regularization parameter. For $\mu' < \mu''$,

$$\text{peak}(\mathbf{u}(\mu''), i) - \text{peak}(\mathbf{u}(\mu'), i) \leq \mu'' - \mu'. \quad (40)$$

This allows to approximate

$$\mu^i = \text{peak}(\mathbf{u}^i, i) \approx \text{peak}(\mathbf{u}^{i-1}, i). \quad (41)$$

This approximation is not limited to a single iteration. Therefore, (41) can be extended further to

$$\mu^i \approx \text{peak}(\mathbf{u}^{i-1}, i) \approx \text{peak}(\mathbf{u}^{i-2}, i) \approx \dots \approx \text{peak}(\mathbf{u}^0, i). \quad (42)$$

This observation motivates the iterative procedure in Table III.

For $i = 0$ there is no previous basis, and the relation (42) is exact. If $(\mathbf{A}^H \mathbf{A})$ were a diagonal matrix, the relation would also be exact. This follows from

$$\begin{aligned} \mathbf{u}^i &= 2\mathbf{D}^{-H} \mathbf{A}^H (\mathbf{y} - \mathbf{A} \mathbf{x}_{\ell_1}^i) \\ &= 2\mathbf{D}^{-H} (\mathbf{A}^H \mathbf{y} - (\mathbf{A}^H \mathbf{A}) \mathbf{x}_{\ell_1}^i). \end{aligned} \quad (43)$$

A diagonal coherence matrix implies the mutual coherence is zero, which is not possible for $M > N$. From (43), it is seen that the coherence matrix of the basis $(\mathbf{A}^H \mathbf{A})$ is re-weighted by the primal solution vector $\mathbf{x}_{\ell_1}^i$ in the i th iteration. The accuracy of the approximation (42) depends on the magnitudes of the off-diagonal elements of the coherence matrix. For discussing the approximation accuracy, note that μ^i depends on the peaks in the magnitude of $|\mathbf{u}^i|$

$$\mathbf{u}^i = 2\mathbf{D}^{-H} \mathbf{A}^H \left(\mathbf{y} - \sum_{m \in \mathcal{M}_i} \mathbf{a}_m \mathbf{x}_{\ell_1, m}^i \right) \quad (44)$$

As long as the *next* active column is orthogonal to *all* active columns \mathbf{a}_m with $m \in \mathcal{M}_i$, the approximation is exact.

Although (44) appears to be quite complicated, Corollary 3 assures that the dual coordinate is linear in the regularization parameter for all $\mu^{*(p+1)} < \mu < \mu^{*p}$. It may happen that the coordinate corresponding to the $(i + 1)$ st peak becomes active first, although $\text{peak}(\mathbf{u}^{i-1}, i) > \text{peak}(\mathbf{u}^{i-1}, i + 1)$. In this case, two sources become active as the regularization parameter is chosen too low. This is not treated in the tables to keep them simple, but this exception can be handled by, e.g., bisection.

B. Dual-based

As asserted by (21), searching for active indices in the dual domain is effectively a form of relaxation of the primal problem (P1'). This amounts to peak finding in the output of a beamformer acting on the residuals, cf. Theorem 1. In line 5, the active set \mathcal{M} is effectively approximated by the relaxed set \mathcal{U}_i .

Instead of the primal (P1'), the dual (18a)–(18c) is solved exclusively. As a demonstrative example, we provide the fast iterative algorithm formulated in the dual domain in Table IV. Note that the gird-free atomic norm solutions [13], [15], [16], [17] follows a solution approach similar to this.

VII. SIMULATION

In this section, the performance of the proposed dual estimation procedures is evaluated based on numerical simulation. We use synthetic data from a uniform linear array with $N = 64$ elements with half-wavelength spacing. The angular domain is discretized by $\theta_m = (m-1)\frac{180^\circ}{M}$ with $m = 1, \dots, M$ and

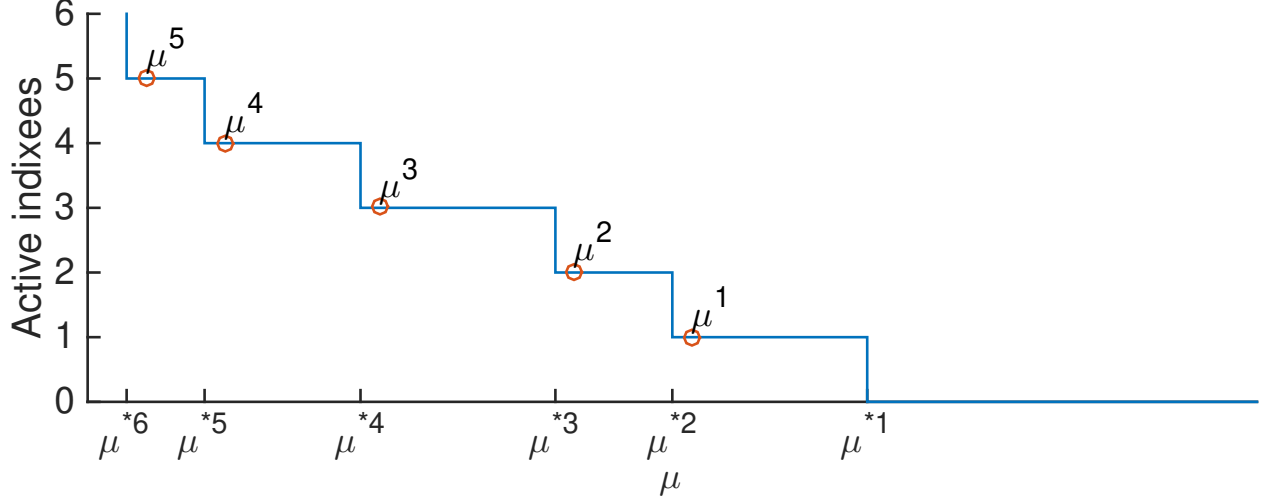


Fig. 10. Illustration of the LASSO path: Number of active indices versus the regularization parameter μ . Increments in the active set occur at μ^{*p}

$M = 180$. The simulation scenario includes $s = 8$ far-field sources modelled by plane waves (28). The uncorrelated noise \mathbf{n} is zero-mean complex-valued circularly symmetric normally distributed $\sim \mathcal{N}(\mathbf{0}, \mathbf{I})$, i.e. 0 dB power. Eight sources are stationary at $\theta^T = [45, 60, 76, 99, 107, 120, 134, 162]$ degrees relative to endfire with constant power level (PL) $[-5, 10, 5, 0, 11, 12, 9, 25]$ dB [21].

The dual solution for the order-recursive approach, Table II, corresponds to the results shown in Fig. 11. The faster iterative approach, Table III, yields the results in Fig. 12. The dual solution using the primal solution from the previous iteration is interpreted as a weighted CBF and used for the selection of μ (left column). Next, the convex optimization is carried out for that value of μ giving the dual solution. We plot the dual solution on a linear scale and normalized to a maximum value of 1 which is customary in implementations of the dual for compressed sensing [13], [15], [16]. The number of active sources (see right column in Figs. 11 and 12) are determined according to line 5 in Tables II and III.

For the order-recursive approach step 1, the μ is selected based on the main peak $\theta = 162^\circ$ and a large side lobe at $\theta = 170^\circ$. The solution progresses steadily down the LASSO path. Figure 12 shows the faster iterative approach in Table III for the 8-source problem. In the first iteration we use a μ between the 8th and 9th peak based on the CBF solution (Fig. 12a). There are many sidelobes associated with the source at $\theta = 162^\circ$. As soon as the dominant source is determined, the sidelobes in the residuals are reduced and only 5 sources are observed. After two more iterations, all 8 sources are found at their correct locations.

Given: $\mathbf{A} \in \mathbb{C}^{N \times M}$, $\mathbf{D} \in \text{diag} \mathbb{R}^M$, $\mathbf{y} \in \mathbb{C}^N$

Given: $s \in \mathbb{N}$, $F \in]0, 1[$.

1: Initialize $i = 0$, $p = 1$, $\mathbf{x}_{\ell_1}^0 = \mathbf{0}$, $\mathbf{u}^0 = 2\mathbf{D}^{-H} \mathbf{A}^H \mathbf{y}$

2: while $p < s$

$i = i + 1$

3: $\mu^i = (1 - F) \text{peak}(\mathbf{u}^{i-1}, i) + F \text{peak}(\mathbf{u}^{i-1}, i + 1)$

4a: $\mathbf{x}_{\ell_1}^i$ = solution to problem (P1') for $\mathbf{A}, \mathbf{D}, \mathbf{y}, \mu = \mu^i$

4b: $\mathbf{u}^i = 2\mathbf{D}^{-H} \mathbf{A}^H (\mathbf{y} - \mathbf{A} \mathbf{x}_{\ell_1}^i)$

5: $\mathcal{M}_i = \{m \mid |x_{\ell_1, m}^i| > \delta_i\}$, $\delta_i = \epsilon \|\mathbf{x}_{\ell_1}^i\|_\infty$
 which ensures that $|\mathcal{M}_i| \leq i$

7: if $|\mathcal{M}_i| < p$

8: $i = i + 1$

9: else

10: $\mathbf{x}_{\ell_0}^p = \mathbf{A}_{\mathcal{M}_i}^+ \mathbf{y}$

11: $\mathcal{M}_p = \mathcal{M}_i$

12: $p = p + 1$

13: end

14: end

15: Output: $\mathbf{x}_{\ell_0}^p, \mathcal{M}_p \quad \forall p = 1 \dots s$

TABLE II

ORDER-RECURSIVE PROCEDURE TO APPROXIMATE (P2).

For both procedures, the main CPU time is used in solving the convex optimization problem. Thus the iterative procedure is a factor 8/3 faster in this case than the straightforward approach which strictly follows the LASSO path. The approach described in Table II has approximately the same CPU time usage as the approach in Ref. [21], but it is conceptually simpler and provides deeper physical insight into the problem.

VIII. CONCLUSION

The complex-valued generalized LASSO problem is strictly convex and strong duality holds. The corresponding dual problem is interpretable as a weighted CBF acting on the residuals of the LASSO.

Given: $\mathbf{A} \in \mathbb{C}^{N \times M}$, $\mathbf{D} \in \text{diag} \mathbb{R}^M$, $\mathbf{y} \in \mathbb{C}^N$	
Given: $s \in \mathbb{N}$, $F \in]0, 1[$	
1:	Initialize $i = 0$, $\mathbf{x}_{\ell_1}^0 = \mathbf{0}$, $\mathbf{u}^0 = 2\mathbf{D}^{-H} \mathbf{A}^H \mathbf{y}$
2:	while $ \mathcal{M}_i < s$ $i = i + 1$
3:	$\mu^i = (1 - F) \text{peak}(\mathbf{u}^{i-1}, s) + F \text{peak}(\mathbf{u}^{i-1}, s + 1)$
4a:	$\mathbf{x}_{\ell_1}^i = \text{solution to problem } (P1')$ for $\mathbf{A}, \mathbf{D}, \mathbf{y}, \mu = \mu^i$
4b:	$\mathbf{u}^i = 2\mathbf{D}^{-H} \mathbf{A}^H (\mathbf{y} - \mathbf{A} \mathbf{x}_{\ell_1}^i)$
5:	$\mathcal{M}_i = \{m \mid x_{\ell_1, m}^i > \delta_i\}$, $\delta_i = \epsilon \ \mathbf{x}_{\ell_1}^i\ _\infty$ which ensures that $ \mathcal{M}_i \leq i$
7:	end
8:	$\mathbf{x}_{\ell_0}^s = \mathbf{A}_{\mathcal{M}_i}^+ \mathbf{y}$
9:	$\mathcal{M}_s = \mathcal{M}_i$
10:	Output: $\mathbf{x}_{\ell_0}^s, \mathcal{M}_s$

TABLE III

ITERATIVE PRIMAL-BASED PROCEDURE TO APPROXIMATE (P2).

There is a linear one-to-one relation between the dual and primal vectors. Any results formulated for the primal problem are readily extendable to the dual problem. Thus, the sensitivity of the primal solution to small changes in the constraints can be easily assessed.

While the LASSO solution gives the \mathbf{x}_{ℓ_1} solution it is usually the \mathbf{x}_{ℓ_0} solution that is of interest. The difference between the \mathbf{x}_{ℓ_0} and the \mathbf{x}_{ℓ_1} is characterized via the dual vector and show its strong linear dependence on the regularization parameter μ and the basis coherence of the active sources, Eq. (26).

Based on mathematical and physical insight, an order-recursive and a faster iterative LASSO-based procedure are proposed and evaluated. These procedures use the dual variable of the generalized LASSO for regularization parameter selection, which greatly facilitates computation of the path as we can predict the changes in the active indexes. Further, a dual-based procedure is formulated which solves only the dual problem. The examples demonstrate the procedures, confirming that the dual and primal coordinates are piecewise linear in the regularization parameter μ .

Given: $\mathbf{A} \in \mathbb{C}^{N \times M}$, $\mathbf{D} \in \text{diag}_{\mathbb{R}}^M$, $\mathbf{y} \in \mathbb{C}^N$

Given: $s \in \mathbb{N}$, $F \in]0, 1[$

1: Initialize $i = 0$, $\mathbf{u}^0 = 2\mathbf{D}^{-H} \mathbf{A}^H \mathbf{y}$

2: while $|\mathcal{M}_i| < s$
 $i = i + 1$

3: $\mu^i = (1 - F) \text{peak}(\mathbf{u}^{i-1}, s) + F \text{peak}(\mathbf{u}^{i-1}, s + 1)$

4: $\mathbf{u}^i = \text{solution to (18a) - (18c) for } \mathbf{A}, \mathbf{D}, \mathbf{y}, \mu = \mu^i$

5: $\mathcal{U}_i = \{m \mid 1 - \frac{|u_m^i|}{\mu} < \epsilon_\mu\}$

6a: $\mathbf{x}_{\ell_0}^i = \mathbf{A}_{\mathcal{U}_i}^+ \mathbf{y}$

6b: $\mathcal{M}_i = \{m \mid |x_{\ell_0, m}^i| > \delta_i\}$, $\delta_i = \epsilon \|\mathbf{x}_{\ell_0}^i\|_\infty$

7: end

8: $\mathbf{x}_{\ell_0}^s = \mathbf{A}_{\mathcal{M}_i}^+ \mathbf{y}$

9: $\mathcal{M}_s = \mathcal{M}_i$

10: Output: $\mathbf{x}_{\ell_0}^s, \mathcal{M}_s$

TABLE IV

ITERATIVE DUAL-BASED PROCEDURE TO APPROXIMATE (P2).

APPENDIX A

Proof of (17): Set $\mathbf{u} = (u_1, u_2, \dots, u_M)^T \in \mathbb{C}^M$.

$$\mu \|\mathbf{z}\|_1 - \text{Re}(\mathbf{u}^H \mathbf{z}) = \sum_{m=1}^M (\mu |z_m| - \text{Re}(u_m^* z_m)) \quad (\text{A1})$$

Further, $u_m^* z_m = |u_m| |z_m| e^{j\phi_{mm}}$, where the phase difference ϕ_{mm} depends on both u_m and z_m . We continue from (A1)

$$= \sum_{m=1}^M \underbrace{(\mu - |u_m| \cos \phi_{mm})}_{\tilde{\mu}_m \geq 0?} |z_m|. \quad (\text{A2})$$

If all coefficients $\tilde{\mu}_m \geq 0$ for all choices $z_m \in \mathbb{C}$ then

$$\min_{\mathbf{z}} (\mu \|\mathbf{z}\|_1 - \text{Re}(\mathbf{u}^H \mathbf{z})) = 0, \quad (\text{A3})$$

otherwise there is no lower bound on the minimum. Therefore, all $|u_m|$ must be bounded, i.e. $|u_m| \leq \mu \forall m = 1, \dots, M$ to ensure that all $\tilde{\mu}_m \geq 0$ for all possible phase differences $-1 \leq \cos \phi_{mm} \leq 1$. Finally, we note that $\|\mathbf{u}\|_\infty = \max_m |u_m|$.

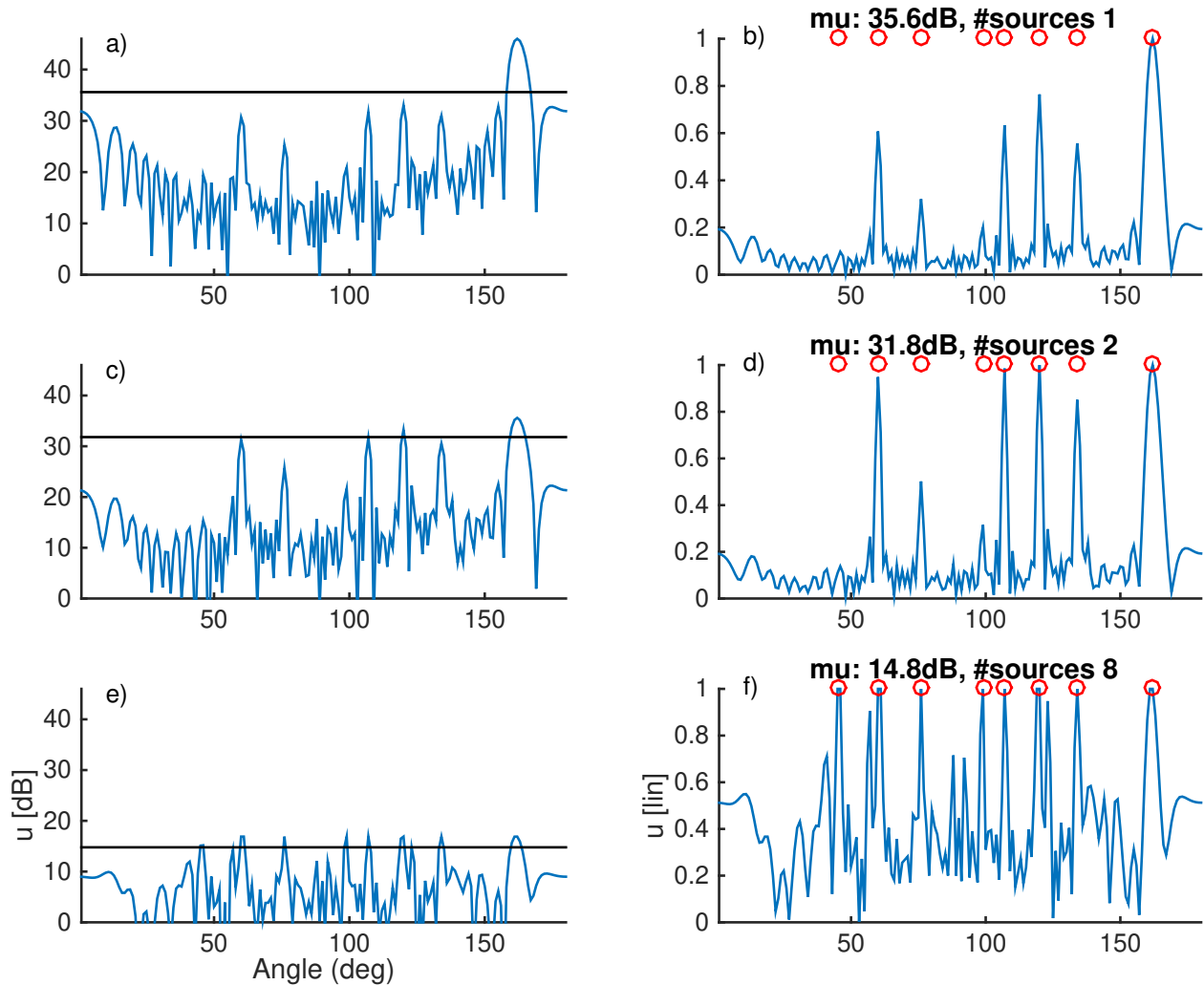


Fig. 11. Dual coordinates for order-recursive approach corresponding to step $p = 1$ (a and b), $p = 2$ (c and d), and $p = 8$ (e and f). Left column: Dual (dB) for the previous step which is used for selecting μ (horizontal line). Right column: Dual (lin) normalized with μ (maximum is 1), the true source locations are marked with \circ , and the actual value of μ and number of sources found is also indicated.

APPENDIX B: PROOFS OF COROLLARIES 1, 2, AND 3

Proof for Corollary 1

Let the objective function of the complex-valued generalized LASSO problem (P1') be

$$\mathcal{L} = \|\mathbf{y} - \mathbf{A}\mathbf{x}\|_2^2 + \mu\|\mathbf{D}\mathbf{x}\|_1. \quad (\text{B1})$$

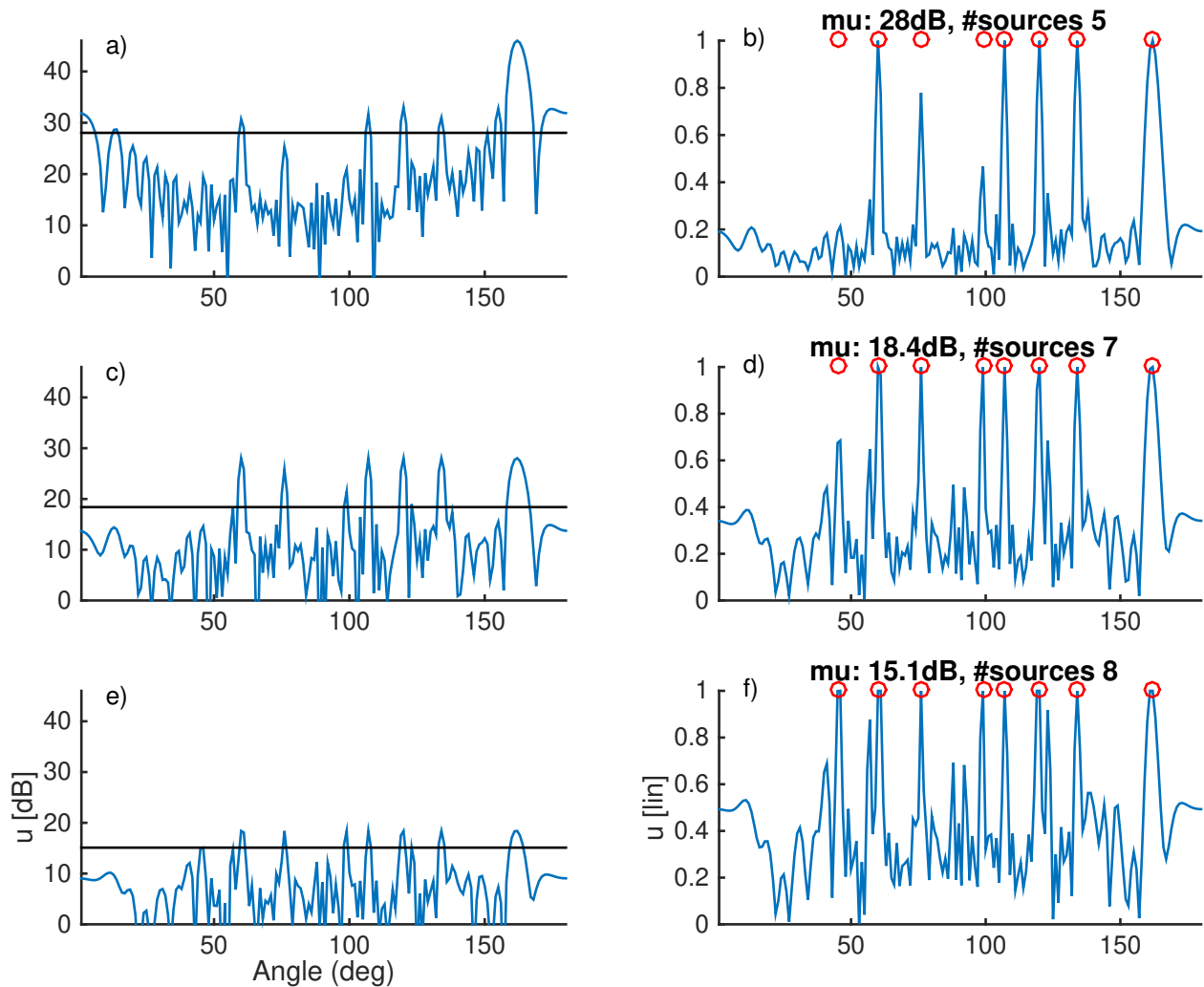


Fig. 12. Dual coordinates iterative approach corresponding for localizing $s = 8$ sources for step $i = 1$ (a and b), $i = 2$ (c and d), and $i = 3$ (e and f). Left column: Dual (dB) for the previous step which is used for selecting μ (horizontal line). Right column: Dual (lin) normalized with μ (maximum is 1), the true source locations are marked with \circ , and the actual value of μ and number of sources found is also indicated..

In the following, we evaluate the subderivative $\partial\mathcal{L}$ [29] as the set of all complex subgradients as introduced in [30]. First, we observe

$$\partial\mathcal{L} = -2\mathbf{A}^H(\mathbf{y} - \mathbf{A}\mathbf{x}) + \mu\partial\|\mathbf{D}\mathbf{x}\|_1. \quad (\text{B2})$$

Next, it is assumed that \mathbf{D} is a diagonal matrix with positive real-valued diagonal entries. It follows that

$$\partial \|\mathbf{D}\mathbf{x}\|_1 = \begin{cases} \frac{D_{mm}^* x_m}{|D_{mm} x_m|} & \text{for } D_{mm} x_m \neq 0 \\ \{z \in \mathbb{C}, |z| \leq 1\} & \text{for } D_{mm} x_m = 0 \end{cases} \quad (\text{B3})$$

The minimality condition for \mathcal{L} is equivalent to setting (B2) to zero. For all m with $D_{mm} x_m \neq 0$ and with (19), this gives

$$\mu \frac{D_{mm}^* x_m}{|D_{mm} x_m|} = u_m . \quad (\text{B4})$$

It readily follows that $|u_m| = \mu$.

Proof for Corollary 2

For matrices \mathbf{D} with positive diagonal entries, we conclude for the active set, $m \in \mathcal{M}$,

$$\mu e^{j \arg(x_m)} = \frac{2}{D_{mm}} \mathbf{e}_m^H \mathbf{A}^H (\mathbf{y} - \mathbf{A}\mathbf{x}) = u_m , \quad (\text{B5})$$

where \mathbf{e}_m is the m th standard basis vector. This concludes the proof of Corollary 2.

Proof for Corollary 3

For the primal vector, this was shown in the real-valued case by Tibshirani [1]. For the complex-valued case, this is a direct consequence of Appendix B in [21]. For the dual vector, this was shown in the real-valued case by Tibshirani [10]. For the complex-valued case, this readily follows from Theorem 1.

APPENDIX C: ℓ_0 SOLUTION

The gradient (cf. Appendix B) of the (P0)– and (P1)–objective functions is

$$\nabla \|\mathbf{y} - \mathbf{A}\mathbf{x}\|_2^2 = -2\mathbf{A}^H (\mathbf{y} - \mathbf{A}\mathbf{x}) \quad (\text{C1})$$

For the active signal components, x_m with $m \in \mathcal{M}$, the ℓ_0 -constraint of (P0) is without effect and the solution results from setting the gradient to zero, i.e. solving the normal equations.

$$\mathbf{A}_{\mathcal{M}}^H \mathbf{y} = \mathbf{A}_{\mathcal{M}}^H \mathbf{A}_{\mathcal{M}} \mathbf{x}_{\ell_0, \mathcal{M}} \quad \Rightarrow \quad \mathbf{x}_{\ell_0, \mathcal{M}} = \mathbf{A}_{\mathcal{M}}^+ \mathbf{y} \quad (\text{C2})$$

We set

$$\mathbf{x}_{\ell_0, \mathcal{M}} = \mathbf{x}_{\ell_1, \mathcal{M}} + \mathbf{\Delta} . \quad (\text{C3})$$

This is inserted into (C1),

$$\nabla \|\mathbf{y} - \mathbf{A}\mathbf{x}_{\ell_1, \mathcal{M}}\|_2^2 = -2\mathbf{A}^H (\mathbf{y} - \mathbf{A}(\mathbf{x}_{\ell_0, \mathcal{M}} - \mathbf{\Delta})). \quad (\text{C4})$$

Using (6) gives

$$2\mathbf{A}_{\mathcal{M}}^H (\mathbf{y} - \mathbf{A}_{\mathcal{M}}\mathbf{x}_{\ell_1, \mathcal{M}}) = \mathbf{D}_{\mathcal{M}}^H \mathbf{u}_{\mathcal{M}} \quad (\text{C5})$$

$$2\mathbf{A}_{\mathcal{M}}^H (\mathbf{y} - \mathbf{A}_{\mathcal{M}}(\mathbf{x}_{\ell_0, \mathcal{M}} - \mathbf{\Delta})) = \mathbf{D}_{\mathcal{M}}^H \mu e^{j\theta_{\mathcal{M}}} \quad (\text{C6})$$

$$2\mathbf{A}_{\mathcal{M}}^H \mathbf{A}_{\mathcal{M}} \mathbf{\Delta} = \mu \mathbf{D}_{\mathcal{M}}^H e^{j\theta_{\mathcal{M}}} \quad (\text{C7})$$

This results in

$$\mathbf{\Delta} = \frac{\mu}{2} (\mathbf{A}_{\mathcal{M}}^H \mathbf{A}_{\mathcal{M}})^{-1} \mathbf{D}_{\mathcal{M}}^H e^{j\theta_{\mathcal{M}}} \quad (\text{C8})$$

which depends on μ both explicitly and implicitly through \mathcal{M} . If the set of nonzero elements of (P0) is equal to the active set of (P1'), the solutions of (P0) and (P1') differ by (C8).

REFERENCES

- [1] R. Tibshirani: Regression Shrinkage and Selection via the Lasso, *J. R. Statist. Soc. B*, vol. 58, no. 1, pp. 267–288, 1996.
- [2] I. F. Gorodnitsky and B. D. Rao: Sparse signal reconstruction from limited data using FOCUSS: A re-weighted minimum norm algorithm, *IEEE Trans. Signal Process.*, vol. 45, no. 3, pp. 600–616, 1997.
- [3] E. J. Candès, J. Romberg, T. Tao: Robust uncertainty principles: Exact signal reconstruction from highly incomplete frequency information, *IEEE Trans. Inf. Theory*, vol. 52, no. 2, pp. 489–509, Feb. 2006.
- [4] D. Donoho: Compressed sensing, *IEEE Trans. Inf. Theory*, vol. 52, no. 4, pp. 1289–1306, Apr. 2006.
- [5] J. J. Fuchs: Recovery of exact sparse representations in the presence of bounded noise, *IEEE Trans. Inf. Theory*, vol. 51, pp. 3601–3608, 2005.
- [6] D. M. Malioutov, C. Mùjdat, A. S. Willsky: A sparse signal reconstruction perspective for source localization with sensor arrays, *IEEE Trans. Signal Process.*, vol. 53, no. 8, pp. 3010–3022, Aug. 2005.
- [7] D. L. Donoho, M. Elad, V. N. Temlyakov: Stable recovery of sparse overcomplete representations in the presence of noise, *IEEE Trans. Inf. Theory*, vol. 52, pp. 6–18, 2006.
- [8] J. A. Tropp: Just relax: Convex programming methods for identifying sparse signals in noise, *IEEE Trans. Inf. Theory*, vol. 52, pp. 1030–1051, 2006.
- [9] M. Elad: *Sparse and Redundant Representations: From Theory to Applications in Signal and Image Processing*, Springer; 2010
- [10] R. J. Tibshirani and J. Taylor: The Solution Path of the Generalized Lasso, *Ann. Statist.*, vol. 39, no. 3, pp. 1335–1371, Jun. 2011.
- [11] S. Fortunati, R. Grasso, F. Gini, M. Greco, and K. LePage: Single-snapshot DOA estimation by using Compressed Sensing, *EURASIP J. Advances in Signal Processing*, Vol 2014, p 120, 2014.
- [12] C. Weiss and A. Zoubir: DOA estimation in the presence of array imperfections: A sparse regularization parameter selection problem, in *Proc. IEEE Workshop on Statistical Signal Processing (SSP)*, pp. 348–351, Gold Coast, Australia, Jun. 29–Jul. 2, 2014.

- [13] G. Tang and B. N. Bhaskar, B.N. P. Shah, B. Recht, Compressed Sensing Off the Grid, *IEEE Transactions on Information Theory*, vol. 59, no. 11, pp. 7465-7490, Nov. 2013
- [14] A. Xenaki, P. Gerstoft and K. Mosegaard: Compressive beamforming, *The Journal of the Acoustical Society of America*, vol. 136, no. 1, pp. 260–271, 2014
- [15] E. J. Candès and C. Fernandez-Granda, Super-resolution from noisy data, *Journal of Fourier Analysis and Applications*, vol. 19, no. 6, pp. 1229–1254, Springer, 2013.
- [16] E. J. Candès and C. Fernandez-Granda, Towards a Mathematical Theory of Super-resolution, *Communications on Pure and Applied Mathematics*, vol. 67, no. 6, pp. 906–956, 2014.
- [17] A. Panahi and M. Viberg: Gridless Compressive Sensing, in *Proc. ICASSP 2014*, Florence, Italy, 2014.
- [18] J. F. de Andrade Jr, M.L.R. de Campos, and J.A. Apolinário Jr.: A complex version of the LASSO algorithm and its application to beamforming, in *Proc. 7th Int. Telecommun. Symp. (ITS 2010)*, Manaus, Brazil, Sep 6–9, 2010.
- [19] D. L. Donoho, Y. Tsaig, I. Drori, J.-L. Starck: Sparse Solution of Underdetermined Systems of Linear Equations by Stagewise Orthogonal Matching Pursuit, *IEEE Transactions on Information Theory*, vol. 58, no. 2, pp.1094–1121, Feb. 2012
- [20] A. Panahi, M. Viberg: Fast LASSO based DOA tracking, in *Proc. Fourth International Workshop on Computational Advances in Multi-Sensor Adaptive Processing (IEEE CAMSAP 2011)*, San Juan, Puerto Rico, Dec. 2011.
- [21] C. F. Mecklenbräuker, P. Gerstoft, A. Panahi, M. Viberg: Sequential Bayesian Sparse Signal Reconstruction Using Array Data, *IEEE Trans. Signal Process.*, vol. 61, no. 24, pp. 6344–6354, Dec. 2013.
- [22] Z. Koldovský, P. Tichavsky, A Homotopy Recursive-in-Model-Order Algorithm for Weighted LASSO, in *Proc. ICASSP 2014*, Florence, Italy, 2014.
- [23] D. Needell and J. A. Tropp, CoSaMP: Iterative signal recovery from incomplete and inaccurate samples, *Appl. Comput. Harmon. Anal.*, vol. 26, pp. 301-321, 2009.
- [24] S. P. Boyd, L. Vandenberghe: *Convex optimization*, Chapters 1–7, Cambridge University Press, 2004.
- [25] S. J. Kim, K. Koh, S. Boyd, D. Gorinevsky, l_1 trend filtering. *SIAM Rev.*, vol. 51, pp. 339–360. MR2505584.
- [26] E. J. Candès, and M. B. Wakin and S. P. Boyd: Enhancing Sparsity by Reweighted l_1 Minimization, *Journal of Fourier Analysis and Applications*, vol. 14, no. 5–6, pp. 877–905, 2008.
- [27] Z. He, S. Xie, S. Ding, A. Cichocki: Convolutional blind source separation in the frequency domain based on sparse representation, *IEEE Trans. Audio, Speech, and Language Proc.*, vol. 15, no. 5, Jul. 2007.
- [28] A. Panahi, M. Viberg: Fast candidate points selection in the LASSO path, *IEEE Signal Process. Lett.*, vol. 19, no. 2, pp. 79–82, Feb. 2012.
- [29] D. P. Bertsekas: *Nonlinear programming*, Athena Scientific, 1999.
- [30] P. Bouboulis, K. Slavakis and S. Theodoridis: Adaptive Learning in Complex Reproducing Kernel Hilbert Spaces Employing Wirtinger’s Subgradients, *IEEE Trans. Neural Networks and Learning Systems*, vol. 23, no. 3, pp.425–438, Mar. 2012.